SINGLE SCAN MR VELOCITY QUANTIFICATION IN ROI BY ALTERNATING VELOCITY ENCODING GRADIENT PULSE POLARITY BETWEEN PHASE ENCODING STEPS

Bremer Jonathan

A thesis submitted to the faculty of the University of North Carolina at Chapel Hill in partial fulfillment of the requirement for the degree of Master in the Department of Biomedical Engineering

Chapel Hill
2008

Approved by:
Dr. Weili Lin
Dr. Brooke Steele
Dr. Carol Lucas

ABSTRACT

Single Scan MR Velocity Quantification in ROI by Alternating Velocity Encoding Gradient Pulse Polarity between Phase Encoding Steps

(Under the direction of Dr. Weili Lin, Dr. Brooke Steele, and Dr. Carol Lucas)

A single scan phase contrast method for quantifying velocity in a region of interest (ROI) containing flowing spins identified prior to scanning is introduced. k-space coverage involves applying positive velocity encoding gradient pulses in acquiring odd phase encoding lines and negative velocity encoding gradient pulses in acquiring even phase encoding lines or vice versa, effectively under sampling flowing spins by a factor of two. A ghost image due to flowing spins in the ROI is formed. The ghost image is located half a field of view away from the ROI in the phase encoding direction. Prior to image acquisition, the field of view in the localizer image is adjusted so that the subsequent ghost image does not overlap with the object being imaged. Velocity quantification is done using image values in ROI and the ghost image. The proposed method is compared to conventional phase contrast in phantom and in vivo. The proposed method reduces scan time considerably.

ACKNOWLEDGEMENTS

I would like to thank my advisors, Dr. Weili Lin, Dr. Brooke Steele and Dr. Carol Lucas, for their support and guidance in this project. I also wish to thank Dr. Robert Dennis for his assistance in making the flow phantom.

I am grateful for the support of my colleagues and friends at the MRI Research Lab at the University of North Carolina. I would like to thank Hongyu, Yasheng, Wei, Ray, Helen and Kathy in particular. Special thanks to Qingwei for the long debates and discussions that helped me hone my ideas.

Finally, I would like to thank my parents for their encouragement and unconditional support.

TABLE OF CONTENTS

I. INTRODUCTION

Phase contrast magnetic resonance imaging (PC MRI or PC) offers a direct way of quantifying flow velocity using MRI. Phase contrast has been described in previous publications [1-3]. Phase contrast has been validated in phantom, animal and human studies [4-19]. Phase contrast relies on the fact that spins moving within a magnetic field gradient acquire phase shift that is proportional to their velocity. To quantify flow in a particular direction two flow encoded scans are required.

Problem Formulation

A sequence of MRI scans (images) that measure blood flow at a given spatial location in a cardiac cycle can be acquired within one cardiac cycle using rapid flow quantification techniques or over several cardiac cycles. These MRI images sample the blood flow profile in time within one cardiac cycle. They are referred to as cardiac phases. Typical rapid blood flow quantification techniques reduce total acquisition time significantly at the expense of low spatial and temporal resolution. Low spatial resolution undermines the accuracy of flow measurements in small vessels [20] where as low temporal resolution means inadequate sampling of the blood flow profile.

Acquiring cardiac phases over several cardiac cycles has the effect of averaging flow measurements over the heart beats and thus prevents the assessment of short term changes in flow patterns that may arise [21]. Also, long acquisition time increase susceptibility to motion artifacts [22]. Motion due to respiration or cardiac activity adversely affects image quality and ultimately flow velocity measurements. Respiratory gating and electrocardiogram (ECG) gating is typically used to compensate for breathing and cardiac motions. However, in patients with cardiac arrhythmias, ECG gating causes significant decay of image quality because of large beat to beat variation. Also, long acquisition time may be difficult for some patients, such as claustrophobic individuals or children. It also means less scans can be performed on any given day.

Aim

The aim of this study is to propose and validate a new phase contrast based method that uses a single scan with a slightly increased field of view to quantify velocity in a region of interest defined in the localizer image[1]. Using a single scan to quantify flow instead of two will reduce acquisition time and improve temporal resolution in the case of rapid flow quantification techniques. Phantom and in vivo studies were conducted to validate the proposed method. In the phantom study, water flow velocity values obtained by phase contrast and the proposed method were compared to water velocity values calculated from pump reading and phantom tube cross section area. In the in vivo study, blood velocity values in the left and right internal carotid arteries (ICA) obtained by the proposed method were compared to blood velocity values in the left and right internal carotid arteries obtained by phase contrast.

[1] A localizer image is a fast low resolution image taken prior to scanning in order to identify the scanning location and configure the field of view appropriately.

II. MRI BACKGROUND

An MRI image is essentially a map of the distribution of nuclear species with non-zero intrinsic angular momentum in an object. Hydrogen atoms, or rather protons, are abundant in the human body. This makes protons the preferred nuclear species imaged in MRI. In MRI the object being imaged is subjected to a strong constant external magnetic field referred to as the $\vec{B_0}$ field. Image contrast, intensity and spatial resolution are achieved through a specific repetitive application of time varying radio frequency magnetic pulses (*rf pulses*) in combination with spatially varying magnetic pulses (*magnetic gradients*). Among other parameters, the time to signal acquisition (TE) and repetition time (TR) are deliberately chosen so as to achieve the desired contrast, image intensity and spatial resolution. This specific combination of TE, TR, rf pulses and magnetic gradients comprise an MRI sequence. There are numerous MRI sequences optimized for specific purposes.

Signal Generation and Detection

MRI principles can be explained adequately in a classical sense even though they have quantum mechanics underpinnings [23]. Protons can be viewed as tiny spinning charges with an attendant circulating electric current. The circulating electric current implies a magnetic dipole moment or simply a magnetic moment ($\vec{\mu}$). In the presence of a constant external magnetic field $\vec{B_0}$ the magnetic moment ($\vec{\mu}$) precesses. The axis of precession is in the direction of $\vec{B_0}$. The precession angular velocity ω_0 is given by $\omega_0 = \gamma\left|\vec{B_0}\right|$ where γ is a constant called the gyromagnetic ratio. This equation is referred to as Larmor equation and the precession frequency is referred to as Larmor frequency. The precession of the magnetic moment implies the presence of torque ($\vec{N}$) in the direction of precession. This in turn implies a time varying angular momentum ($\vec{J}$) often referred to as spin. The torque $\vec{N}$ is given by $\vec{N} = \vec{\mu} \times \vec{B_0}$. Experiments show that angular momentum (spin) is directly related to the magnetic moment $\vec{\mu}$. This relationship is given by $\vec{\mu} = \gamma\vec{J}$. Thus, the expression for torque on a proton due to an external magnetic field $\vec{B_0}$ is given by $\frac{d\vec{\mu}}{dt} = \gamma\vec{\mu} \times \vec{B_0}$. This equation is known as

the equation of motion. In MRI, it is instructive to speak of the angular momentum of protons (spins) than the protons themselves.

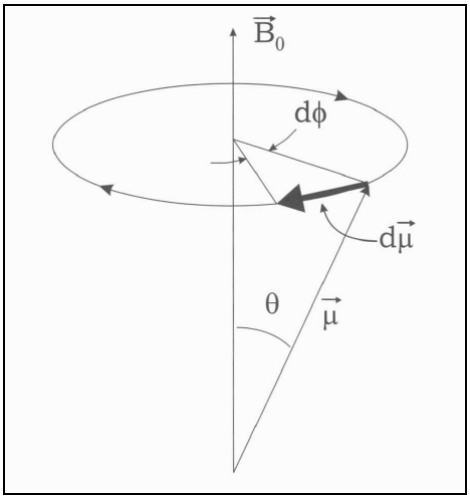

FIG. 1. Precession of magnetic moment $\vec{\mu}$ in the presence of external magnetic field $\vec{B_0}$.

Thermal energy kT, where k is the Boltzmann's constant and T the absolute temperature, prevent the magnetic moment vector of a proton $\vec{\mu}$ from fully relaxing to an alignment along $\vec{B_0}$. The thermal energy is millions of times larger than the quantum energy difference for parallel alignment (lower energy) versus anti-parallel alignment (higher energy) in human body temperature. However, the number of spins parallel to the magnetic field exceeds the number anti-parallel to that field. This spin excess is very small. For instance, the spin excess is only one in a million spins even for a magnetic field strength as large as 0.3T [23]. Although spin excess is extremely small compared to the total number of proton spins, it is enough to produce significant signal that is detectable at room temperature.

In practice it is instructive to talk of the magnetic moment vector density due to proton population $\vec{M}$ (i.e. magnetization vector) in place of the magnetic moment vector $\vec{\mu}$ of a single proton. Essentially substituting $\vec{\mu}$ with $\vec{M}$ in the equation of motion. $\vec{M}$ must be tipped away from $\vec{B}_0$ and into the transverse plan in order to yield detectable changing magnetic flux (signal) in receiver coil of the MRI scanner. It turns out that the solution to the equation of motion shows that a burst of a weak radiofrequency magnetic field known as an rf pulse, applied orthogonally to $\vec{B}_0$ is maximally synchronized to tip $\vec{M}$ when its radiofrequency is tuned to the Larmor frequency. The rf pulse is transmitted by a transmitter coil.

Spatial Encoding

2D slice excitation or selection involves generating signal from a layer of thickness Δz by tipping magnetization in that layer to the transverse plan. This is done by applying an rf pulse with finite bandwidth centered at the Larmor frequency of the spins experiencing the combined effect of a constant external magnetic field $\vec{B}_0$ field and a spatially varying magnetic field known as gradient field. The static field $\vec{B}_0$ is always on. If $\vec{B}_0$ is in the z direction and is given by $\vec{B}_0 = B_0\vec{z}$ and a linear gradient field in z given by $\vec{B}(z) = Gz\vec{z}$ is switched on, the total magnetic field along z becomes $\vec{B}_0 + \vec{B}(z) = (B_0 + Gz)\vec{z}$. The Larmor frequency ω of spins will vary along z and is given by $\omega = \gamma B_0 + \gamma Gz$. This means a slice of thickness Δz at $z = z_0$ is excited by an rf pulse whose frequency ω is centered at $\omega = \gamma(B_0 + G_z z_0)$ and has bandwidth BW_{rf} equal to $BW_{rf} = \gamma G_z(\Delta z)$. The rf pulse and the gradient have to be on at the same time during slice selection. The direction orthogonal to the slice (z in this case) is referred to as the slice select direction.

After slice selection the rf pulse and gradient along z are off and the spins in the selected slice are now precessing in the transverse plane (xy plane) at $\omega_0 = \gamma B_0$. The signal is detected by turning on the receiver coil. The time from rf pulse application (slice selection) to signal detection is the echo time (TE). The signal from a spin at location (x,y) in the selected slice can be modeled as having magnitude $I(x, y)$ and phase $\Omega(x, y) = -\omega_0 t = -\gamma B_0 t$. In other words $I(x, y)$ is the image value at (x,y). At this point in time the signal picked up by the receiver coil is coming from the entire population of spins precessing at Larmor frequency ($\omega_0 = \gamma B_0$) in the selected slice. The detected signal $s(t)$ is therefore the sum of all image values $I(x, y)e^{i\Omega(x,y)}$ in the selected slice and is thus given by $s(t) = \iint I(x, y)e^{i\Omega(x,y)}dxdy$.

Adding a linear magnetic gradient field $\vec{B}(x) = Gx\vec{x}$ along x creates a relationship between spin precession frequency ω and the x position. This relationship is given by $\omega = \gamma B_0 + \gamma Gx$. The signal received in the presence of the gradient field $\vec{B}(x)$ is given by $s(t) = \iint I(x, y)e^{i(\Omega(x,y)+\theta(x,y))}dxdy$ where $\Omega(x, y) = -\omega_0 t = -\gamma B_0 t$ and $\theta(x, y) = -\gamma Gxt$. Demodulating the signal with frequency equal to Larmor frequency ω_0 then low pass filtering it makes $\Omega(x, y) = 0$ and the signal is now given by $s(t) = \iint I(x, y)e^{i\theta(x,y)}dxdy = \iint I(x, y)e^{-i\gamma G_x xt}dxdy$. This process of establishing a relationship between the

position of spins (along x in this instance) and their frequency of precession is referred to as frequency encoding. Substituting $k_x = k_x(t) = \frac{\gamma}{2\pi} G_x t$ into the signal equation changes the signal equation to $s(k_x) = \iint I(x, y) e^{-i2\pi k_x x} dxdy$. It becomes apparent that the signal $s(k_x)$ is the Fourier transform of image values $I(x,y)$ along x. Signal $s(k_x)$ is said to be in k-space domain and it is what is detected by the receiver coil of the MRI scanner. The image values $I(x,y)$ along x can be determined by calculating the inverse Fourier transform of the signal s(k_x) which gives $\int I(x, y) dy = \int s(k_x) e^{i2\pi k_x x} dk_x$. $\int I(x, y) dy$ is a 1D image in which all image values along y at a given x location are projected (summed up) onto x. The calculated image values $I(x, y)$ are resolved in x but not in the y direction. In order to resolve $I(x, y)$ in y the signal equation s(k_x) needs to be in 2D. Incorporating another dimension in k-space (k_y) into the signal equation changes it to $s(k_x, k_y) = \iint I(x, y) e^{-i2\pi k_x x} e^{-i2\pi k_y y} dxdy$ where $k_x = k_x(t) = \frac{\gamma}{2\pi} G_x t$ and $k_y = k_y(t) = \frac{\gamma}{2\pi} G_y t$.

In practice 2D signal acquisition involves sampling k-space in 2D. First the desired slice location is selected as describe before, then the selected slice is phase encoded then frequency encoded. This process is repeated until the entire k-space is covered. The time between consecutive rf pulses is the repetition time (TR). Phase encoding involves sampling a k_y value at which k_x values or rather the 1D s(k_x) signal desired above is detected (i.e. frequency encoded and sampled simultaneously). In fact, the 1D signal s(k_x) described earlier is signal acquired at $k_y = 0$. If the sampling steps in k_x and k_y are Δk_x and Δk_y respectively, the discrete version of the signal equation is given by $s(m\Delta k_x, n\Delta k_y) = \sum_{q=-\infty}^{\infty} \sum_{p=-\infty}^{\infty} I(p\Delta x, q\Delta y) e^{-i2\pi m\Delta k_x p\Delta x} e^{-i2\pi n\Delta k_y q\Delta y}$. The corresponding image equation is given by $I(p\Delta x, q\Delta y) = \sum_{n=-\infty}^{\infty} \sum_{m=-\infty}^{\infty} s(m\Delta k_x, n\Delta k_y) e^{-i2\pi m\Delta k_x p\Delta x} e^{-i2\pi n\Delta k_y q\Delta y}$. The direction in which slice selection is performed (in this case z direction) is known as the slice select direction (SS) whereas the direction in which phase encoding is performed (in this case y direction) is known as the phase encoding direction (PE) and the direction in which frequency encoding is performed (in this case the x direction) is known as the readout direction (RO).

Relaxation Times and Image Contrast

Magnetization in the transverse plane tends to grow back along the direction of the static field $\overrightarrow{B_0}$. This causes signal decay. The rate of magnetization regrowth is characterized by a time constant T_1 called the longitudinal relaxation time. T_1 decay arises from the interaction between the spins and the atomic neighborhood. T_1 decay is also known as the spin-lattice decay. Signal decay is also brought about by spin to spin interaction. Spin to spin interaction leads to dephasing of spins in the transverse plane. This dephasing of spins is due to variations of local precession frequencies. The spin to spin relaxation (decay) time is modeled by a time constant T_2. External magnetic field inhomogeneities bring about further spin dephasing which in effect shortens T_2 further. This shorter T_2 is referred to as T_2^*.

Contrast between different tissues in MRI arises from the fact that T_1, T_2 and spin density values are tissue dependent. T_1, T_2 or spin density weighted images are generated by manipulating echo time (TE) and repetition time (TR).

Phase Contrast Velocity Encoding

Velocity encoding (quantification) in a particular direction is done by adding a bipolar gradient pulse in that direction. Prior to velocity encoding motion artifacts are minimized by employing velocity compensation techniques [23]. A bipolar gradient pulse is composed of two magnetic gradient pulses of equal duration and magnitude but opposite polarity. A bipolar gradient pulse is said to be positive if it constitutes the positive gradient pulse first followed by the negative gradient pulse. A negative bipolar gradient pulse constitutes the negative gradient pulse first followed by the positive gradient pulse. Spins flowing in the direction of a positive bipolar gradient pulse develop phase angle $\theta = -\gamma G \upsilon \tau^2$ (where γ is the gyromagnetic ratio constant for a proton, G is the magnitude of the bipolar gradient pulse, υ is spin's flow velocity and τ is the duration of the bipolar gradient pulse). Incorporating velocity encoding to image values $I(p\Delta x, q\Delta y)$ results in $I(p\Delta x, q\Delta y)e^{i\theta(p\Delta x, q\Delta y)}$ where $I(p\Delta x, q\Delta y)$ is the image value at $(p\Delta x, q\Delta y)$ and $\theta(p\Delta x, q\Delta y)$ is phase due to velocity at that location. $\theta(p\Delta x, q\Delta y) = 0$ for stationary spins (tissue).

The phase image derived from the acquired image may have spurious errors due to field inhomogeneities or rf penetration effects [23]. These background phase errors are independent of the bipolar gradient pulse and can be eliminated. The background phase errors which are constant or rather vary slowly throughout image

acquisition are removed by acquiring velocity compensated scans in pairs; a positive velocity encoded scan and a negative velocity encoded scan. A positive bipolar gradient pulse is applied in acquiring the positive velocity encoded scan and negative bipolar gradient pulse is applied in acquiring the negative velocity encoded scan. The phase angle due to flow in the positive velocity encoded scan is given by $\theta_{+}(p\Delta x, q\Delta y) = -\gamma G\upsilon(p\Delta x, q\Delta y)\tau^2$ whereas in the negative velocity encoded scan the phase angle is given by $\theta_{-}(p\Delta x, q\Delta y) = \gamma G\upsilon(p\Delta x, q\Delta y)\tau^2 = -\theta_{+}(p\Delta x, q\Delta y)$. Subtracting the positive velocity encoded phase image from the negative velocity encoded phase image removes any constant background phase errors while doubling the velocity induced phase angle in the resulting phase difference image. Random phase errors which are usually small can be minimized through averaging repeated acquisitions.

The G and τ values of the bipolar gradient pulse need to be selected such that $|\theta(p\Delta x, q\Delta y) = \gamma G\upsilon(p\Delta x, q\Delta y)\tau^2| < \pi$ because the phase angle range is from $-\pi$ to π. Any angle less than $-\pi$ or greater than π will be folded (aliased) between $-\pi$ and π. In practice, the maximum possible velocity expected is assumed prior to velocity measurements. This velocity is known as the encoding velocity (υ_{enc}). Parameters G and τ are set such that υ_{enc} produces a velocity induced phase angle of π (Eq. (1)).

$$\pi = \gamma G\upsilon_{enc}\tau^2 \tag{1}$$

Thus, velocity at image (pixel) location $(p\Delta x, q\Delta y)$ is given by:

$$\upsilon(p\Delta x, q\Delta y) = \frac{\theta(p\Delta x, q\Delta y)}{\pi} \times \upsilon_{enc} \tag{2}$$

Quantifying velocity this way is called Phase Contrast Magnetic Resonance Imaging (PC-MRI or PC in short). It requires scans to be acquired in pairs.

III. PROPOSED VELOCITY QUANTIFICATION METHOD

This chapter provides the theory behind the proposed method of quantifying velocity by alternating the polarity of the bipolar gradient pulse between phase encoding steps. The *Even and Odd Image Decomposition* section derives the image equation of images reconstructed using even and odd phase encoding lines. The *Velocity Quantification* section derives the image equation of images reconstructed using positive velocity encoded even phase encoding lines and negative velocity encoded odd phase encoding lines. The *Determining Velocity* section describes a way to determine velocity using the proposed method. The *Flow Direction Distinction* section describes a way to distinguish flow in opposite direction.

Even and Odd Image Decomposition

If the 2D MR signal of an L_x by L_y slice is given by $s(m,n)$ [2] then the image $I(p,q)$ [3] reconstructed from $s(m,n)$ is given by: $I(p,q) = F^{-1}(s(m,n))$ where m and n are k-space domain matrix indices, p and q are image domain matrix indices, L_x and L_y correspond to readout and phase encoding image dimensions respectively, and F^{-1} is the Inverse Discrete Fourier Transform. Image $I(p,q)$ can be expressed as $I(p,q) = I_e(p,q) + I_o(p,q)$, where $I_e(p,q)$ is the image reconstructed using even rows (i.e. even phase encoding lines) of the $s(m,n)$ and $I_o(p,q)$ is the image reconstructed using odd rows (i.e. odd phase encoding lines) of $s(m,n)$. $I_e(p,q)$ and $I_o(p,q)$ are given by:

$$I_e(p,q) = F^{-1}(s(m,n) \times u_e(k_x,k_y)) = F^{-1}(s(m,n)) \otimes F^{-1}(u_e(k_x,k_y)) \tag{3}$$

$$I_o(p,q) = F^{-1}(s(m,n) \times u_o(k_x,k_y)) = F^{-1}(s(m,n)) \otimes F^{-1}(u_o(k_x,k_y)) \tag{4}$$

Where $\otimes$ is the convolution operator, k_x and k_y are continuous k-space variables in the readout and phase encoding direction respectively. $u_e(k_x, k_y)$ is a function that samples even rows of $s(m,n)$ and $u_o(k_x,k_y)$ is a function that samples odd rows of $s(m,n)$. $F^{-1}(u_e(k_x,k_y))$ and $F^{-1}(u_o(k_x,k_y))$ are given by:

---

[2] $s(m,n)$ is shorthand for $s(m\Delta k_x, n\Delta k_y)$

[3] $I(p,q)$ is shorthand for $I(p\Delta x, q\Delta y)$

$$U_e(p,q) = F^{-1}(u_e(k_x,k_y)) = F^{-1}(\Delta k_x \Delta k_y \sum_{n=0}^{N}\sum_{m=0}^{M} \delta(k_x - m\Delta k_x, k_y - 2n\Delta k_y)) \\ = \frac{1}{2}\sum_{h=-\infty}^{\infty}\sum_{g=-\infty}^{\infty} \delta(p - gL_x, q - h\frac{L_y}{2}) \tag{5}$$

$$U_o(p,q) = F^{-1}(u_o(k_x,k_y)) = F^{-1}(\Delta k_x \Delta k_y \sum_{n=0}^{N}\sum_{m=0}^{M} \delta(k_x - m\Delta k_x, k_y - (2n+1)\Delta k_y)) \\ = \frac{1}{2}\sum_{h=-\infty}^{\infty}\sum_{g=-\infty}^{\infty} \delta(p - gL_x, q - h\frac{L_y}{2}) e^{ih\pi} \tag{6}$$

From Eq. (3), Eq. (4), Eq. (5) and Eq. (6), $I_e(p,q)$ and $I_o(p,q)$ are given by:

$$I_e(p,q) = I(p,q) \otimes U_e(p,q) = \frac{1}{2}\sum_{h=-\infty}^{\infty}\sum_{g=-\infty}^{\infty} I(p - gL_x, q - h\frac{L_y}{2}) \tag{7}$$

$$I_o(p,q) = I(p,q) \otimes U_o(p,q) = \frac{1}{2}\sum_{h=-\infty}^{\infty}\sum_{g=-\infty}^{\infty} I(p - gL_x, q - h\frac{L_y}{2}) e^{ih\pi} \tag{8}$$

From Eq. (7) and Eq. (8) we see that $I_e(p,q)$ and $I_o(p,q)$ is a series of the images $I(p,q)$ scaled by ½, and repeating every L_x in the x (i.e. readout) direction and every $L_y/2$ in the y (i.e. phase encoding) direction. Additionally, for $I_o(p,q)$, the sign alternates between the repeating $I(p,q)$ images in the y direction. Because the field of view is L_x by L_y, the repeating images for which $|g| \geq 1$ and $|h| > 1$ do not appear in the image because they fall outside the field of view. Hence, Eq. (7) and Eq. (8) reduce to Eq. (9) and Eq. (10) respectively. Note that adding Eq. (9) to Eq. (10) gives $I(p,q)$.

$$I_e(p,q) = \frac{1}{2}I(p, q + \frac{L_y}{2}) + \frac{1}{2}I(p,q) + \frac{1}{2}I(p, q - \frac{L_y}{2}) \tag{9}$$

$$I_o(p,q) = -\frac{1}{2}I(p, q + \frac{L_y}{2}) + \frac{1}{2}I(p,q) - \frac{1}{2}I(p, q - \frac{L_y}{2}) \tag{10}$$

During velocity encoding, the phase angle $\theta(p,q)$ at (p,q) due to moving spins at that location is given by $\theta(p,q) = -\gamma G \upsilon(p,q) \tau^2$ (γ is the gyromagnetic ratio constant for a spin, G is the magnitude of the bipolar gradient pulse, $\upsilon(p,q)$ is the velocity of the spin at (p,q) and τ is the duration of the bipolar gradient pulse). The image equation becomes $I(p,q)e^{i\theta(p,q)}$ where $I(p,q)$ is the image value at (p,q) without velocity encoding and $\theta(p,q)$ is the phase angle value at (p,q) due to velocity. $\theta = 0$ for stationary spins (tissue). Therefore, with velocity encoding, $I_e(p,q)$ and $I_o(p,q)$ become:

$$I_e(p,q) = \frac{1}{2}I(p, q + \frac{L_y}{2}) e^{i\theta(p, q + \frac{L_y}{2})} + \frac{1}{2}I(p,q)e^{i\theta(p,q)} + \frac{1}{2}I(p, q - \frac{L_y}{2}) e^{i\theta(p, q - \frac{L_y}{2})} \tag{11}$$

$$I_o(p,q) = -\frac{1}{2}I(p,q+\frac{L_y}{2})e^{i\theta(p,q+\frac{L_y}{2})} + \frac{1}{2}I(p,q)e^{i\theta(p,q)} - \frac{1}{2}I(p,q-\frac{L_y}{2})e^{i\theta(p,q-\frac{L_y}{2})} \quad (12)$$

The sign of $\theta(p,q)$ changes when the polarity of the bipolar gradient pulse changes because $\theta(p,q)$ is given by $-\gamma G\upsilon(p,q)\tau^2$. It should be noted that the sign of $\theta(p,q)$ also changes when the sign of velocity ($\upsilon(p,q)$) changes in responses to change in flow direction. Thus, changing the bipolar gradient pulse polarity will change the image from $I(p,q)e^{i\theta(p,q)}$ to $I(p,q)e^{-i\theta(p,q)}$. Subsequently, $I_e(p,q)$ and $I_o(p,q)$ become:

$$I_e(p,q) = \frac{1}{2}I(p,q+\frac{L_y}{2})e^{-i\theta(p,q+\frac{L_y}{2})} + \frac{1}{2}I(p,q)e^{-i\theta(p,q)} + \frac{1}{2}I(p,q-\frac{L_y}{2})e^{-i\theta(p,q-\frac{L_y}{2})} \quad (13)$$

$$I_o(p,q) = -\frac{1}{2}I(p,q+\frac{L_y}{2})e^{-i\theta(p,q+\frac{L_y}{2})} + \frac{1}{2}I(p,q)e^{-i\theta(p,q)} - \frac{1}{2}I(p,q-\frac{L_y}{2})e^{-i\theta(p,q-\frac{L_y}{2})} \quad (14)$$

Velocity Encoding

Let $\hat{I}(p,q)$ be the resulting image obtained from taking 2D Inverse Discrete Fourier Transform of the acquired signal matrix $s(m,n)$. $\hat{I}(p,q)$ can be expressed as the sum of $I_e(p,q)$ and $I_o(p,q)$ where $I_e(p,q)$ is the image reconstructed using even rows of $s(m,n)$ while setting the odd rows to zero and $I_o(p,q)$ is the image reconstructed using odd rows of $s(m,n)$ while setting the even rows to zero. Assuming that positive bipolar gradient pulses were applied in acquiring even rows of $s(m,n)$ and negative bipolar gradient pulses were applied in acquiring the odd rows, $I_e(p,q)$ and $I_o(p,q)$ are expressed as:

$$I_e(p,q) = \frac{1}{2}I(p,q+\frac{L_y}{2})e^{i\theta(p,q+\frac{L_y}{2})} + \frac{1}{2}I(p,q)e^{i\theta(p,q)} + \frac{1}{2}I(p,q-\frac{L_y}{2})e^{i\theta(p,q-\frac{L_y}{2})} \quad (15)$$

$$I_o(p,q) = -\frac{1}{2}I(p,q+\frac{L_y}{2})e^{-i\theta(p,q+\frac{L_y}{2})} + \frac{1}{2}I(p,q)e^{-i\theta(p,q)} - \frac{1}{2}I(p,q-\frac{L_y}{2})e^{-i\theta(p,q-\frac{L_y}{2})} \quad (16)$$

$I(q,p)$ is the image that would have resulted without velocity encoding (i.e. no bipolar gradient pulse applied), $\theta(p,q)$ is the phase angle due to velocity, L_y and L_x are image dimensions in phase encoding and readout directions respectively. $\theta(p,q)$ is given by $\theta(p,q) = -\gamma G\upsilon(p,q)\tau^2$ where γ is the gyromagnetic ratio constant for a proton, G is the magnitude of the bipolar gradient pulse, $\upsilon(p,q)$ is the spin's velocity at location (p,q) and τ is the duration of the bipolar gradient pulse. Adding Eq. (15) to Eq. (16) gives:

$$\hat{I}(p,q) = I(p,q+\frac{L_y}{2})\sin\theta(p,q+\frac{L_y}{2}) + I(p,q)\cos\theta(p,q) + I(p,q-\frac{L_y}{2})\sin\theta(p,q-\frac{L_y}{2}) \quad (17)$$

FIG. 2 offers a visual representation of Eq. (17). In FIG. 2, the red circle represents a region of interest where there is flow. If (p_o,q_o) represent coordinates inside the red circle, then image values inside the red circle

are given by Eq. (18). Eq. (18) comes from substituting (p,q) with (p_o,q_o) in Eq. (17). The $I(p_o,q_o-L_y/2)\sin\theta(p_o,q_o-L_y/2)$ term is dropped in Eq. (18) because the coordinates $(p_o,q_o-L_y/2)$ are in fact located outside the image field of view since $q_o-L_y/2 < -L_y/2$ because $-L_y/2 < q_o < 0$.

$$\hat{I}(p_o,q_o) = I(p_o,q_o+\frac{L_y}{2})\sin\theta(p_o,q_o+\frac{L_y}{2}) + I(p_o,q_o)\cos\theta(p_o,q_o) \tag{18}$$

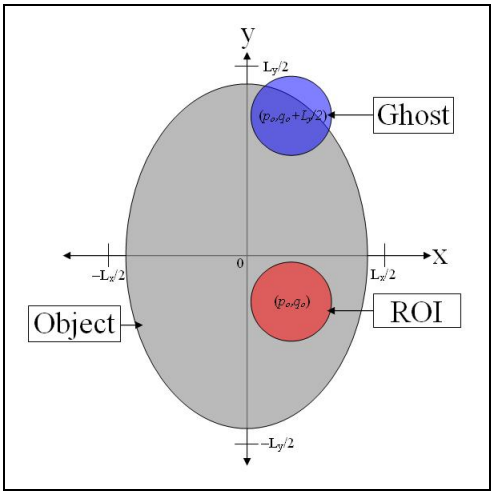

FIG. 2. Visual representation of Eq. (17). The red circle represents a region of interest where there is flow. The purple circle represents the corresponding ghost image due to flow in the red circle. In this field of view configuration the ghost image overlays the object.

The image values at image location $(p_o,q_o+L_y/2)$ are given by Eq. (19). Eq. (19) comes from plugging coordinates $(p_o,q_o+L_y/2)$ in Eq. (17). Likewise, the $I(p_o,q_o+L_y)\sin\theta(p_o,q_o+L_y)$ term is dropped in Eq. (19) because location (p_o,q_o+L_y) is in fact outside the image field of view since $q_o+L_y > L_y/2$ because $-L_y/2 < q_o < 0$.

$$\hat{I}(p_o,q_o+\frac{L_y}{2}) = I(p_o,q_o+\frac{L_y}{2})\cos\theta(p_o,q_o+\frac{L_y}{2}) + I(p_o,q_o)\sin\theta(p_o,q_o) \tag{19}$$

Determining Velocity

Assuming that there are no flowing spins at $(p_o,q_o+L_y/2)$ (i.e. $\theta(p_o,q_o+L_y/2) = 0$), Eq. (18) and (19) reduce to Eq. (20) and (21). The $I(p_o,q_o)\sin\theta(p_o,q_o)$ term in Eq. (21) represents flow ghost values which are overlaid onto the image values at $(p_o,q_o+L_y/2)$ given by the $I(p_o,q_o+L_y/2)$ term.

$$\hat{I}(p_o,q_o) = I(p_o,q_o)\cos\theta(p_o,q_o) \tag{20}$$

$$\hat{I}(p_o,q_o+\frac{L_y}{2}) = I(p_o,q_o+\frac{L_y}{2}) + I(p_o,q_o)\sin\theta(p_o,q_o) \tag{21}$$

$\theta(p_o,q_o)$ which is the phase angle at (p_o,q_o) due to flow, is given by Eq. (22). $I(p_o,q_o+L_y/2)$ is the image value at $(p_o,q_o+L_y/2)$ prior to the overlaid flow ghost.

$$\theta(p_o,q_o) = \tan^{-1}\left(\frac{|\hat{I}(p_o,q_o+\frac{L_y}{2}) - I(p_o,q_o+\frac{L_y}{2})|}{|\hat{I}(p_o,q_o)|}\right) \tag{22}$$

$\theta(p_o,q_o)$ cannot be resolved because it is impossible to determine $I(p_o,q_o+L_y/2)$ in Eq. (22). However, by orienting the region of interest containing flow (i.e. red circle) relative to the field of view as in FIG. 3, image location $(p_o,q_o+L_y/2)$ falls outside object boundaries thus making $I(p_o,q_o+L_y/2) \approx 0$. Eq. (21) becomes Eq. (23) and $\theta(p_o,q_o)$ can now be determined using Eq. (24).

$$\hat{I}(p_o,q_o+\frac{L_y}{2}) \approx I(p_o,q_o)\sin\theta(p_o,q_o) \tag{23}$$

$$\theta(p_o,q_o) \approx \tan^{-1}\left(\frac{|\hat{I}(p_o,q_o+\frac{L_y}{2})|}{|\hat{I}(p_o,q_o)|}\right) \tag{24}$$

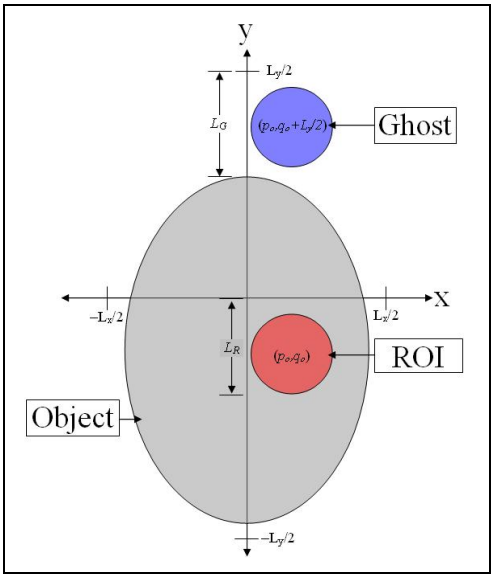

FIG. 3. Visual representation of Eq. (17). The red circle represents a region of interest where there is flow. The purple circle represents the corresponding ghost image due to flow in the red circle. In this field of view configuration the ghost image does not overlay the object.

MRI flexibility allows for the field of view to be easily configured as in FIG. 3. This is done by rotating, translating and increasing the field of view in the localizer as desired. The field of view in FIG. 3 is obtained by having the region of interest containing flow (i.e. red circle) right below the y = 0 line and having length $L_R = L_G$. Eq. (25) uses $\theta(p_o,q_o)$ to calculate flow velocity at image location (p_o,q_o).

$$\upsilon(p_o, q_o) = \frac{\theta(p_o, q_o)}{\pi} \times \upsilon_{\text{enc}} \tag{25}$$

Flow Direction Distinction

Eq. (26) derived from Eq. (20) and Eq. (23) provides a way to distinguish velocities in opposite directions. $\Theta(p_o,q_o)$ is the argument of the ratio between $\hat{I}(p_o,q_o+L_y/2)$ and $\hat{I}(p_o,q_o)$ as given by Eq. (20) and Eq. (23) respectively. If as result of velocity in a particular direction $\theta(p_o,q_o)$ is positive, then $\Theta(p_o,q_o)$ is approximately zero or $\pm 2\pi$. However, if $\theta(p_o,q_o)$ is negative due to velocity in the opposite direction, $\Theta(p_o,q_o)$ becomes approximately $\pm\pi$ because $\hat{I}(p_o,q_o+L_y/2) \approx I(p_o,q_o)\sin(-\theta(p_o,q_o)) = -I(p_o,q_o)\sin\theta(p_o,q_o)$.

$$\Theta(p_o, q_o) = \text{Arg}\left(\frac{\hat{I}(p_o, q_o + \frac{L_y}{2})}{\hat{I}(p_o, q_o)}\right) \approx 0 \text{ or } \pm\pi \tag{26}$$

IV. METHODS AND MATERIALS

This chapter provides a description of experiments conducted to validate the proposed method and demonstrate the reduction in acquisition time. The *MRI Sequence* section outlines the implementation of the phase contrast and proposed method sequences. The *Flow Phantom Study* section describes the flow phantom study used to validate phase contrast and the proposed methods. In the *In vivo study* section, blood velocity values in the left and right internal carotid arteries of seven volunteers obtained by the proposed method and phase contrast were compared. Phase contrast blood velocity values were taken as the gold standard. The *Image Processing* section describes the image-processing tool used to process raw MRI data retrieved from scan.

MRI Sequence

All studies were conducted in a Siemens MAGNETOM Allegra 3T scanner (Siemens, Erlangen, Germany). Phase contrast and proposed method magnetic resonance sequences were implemented by adding bipolar gradient pulses in the slice select direction to a velocity compensated gradient echo sequence (GRE) provided by Siemens. The bipolar gradient pulse was designed to have minimum duration (i.e. minimum τ and τ_r in $\pi = \gamma G \upsilon_{enc}(\tau+\tau_r)(\tau+2\tau_r)$) by setting the amplitude of the bipolar gradient pulse (G) to the maximum value allowed by the system (G=16mT/m) and using the fastest rise and fall times (τ_r=100μs) of the maximum gradient amplitude. Consequently the encoding velocity υ_{enc} had an upper limit of 1894.16cm/s beyond which the flattop time (τ) given by solving equation ($\pi = \gamma G \upsilon_{enc}(\tau+\tau_r)(\tau+2\tau_r)$) becomes negative and thus unacceptable.

A graphical user interface control called special card was added to the sequence's graphical user interface also known as protocol interface. The special card had a dropdown menu with phase contrast and proposed method options, and a text field for setting the encoding velocity (υ_{enc}) value. Maximum υ_{enc} allowed was set to 1894.16cm/s. The phase contrast option sets the number of scans acquired in a single acquisition to two. These two scans are acquired in an interleaved manner where the polarity of the bipolar gradient pulse is alternated between them. That is, assuming one phase encoding line is acquired at a time, the first phase encoding line of the first scan is acquired first with a positive bipolar gradient pulse applied, followed by the first phase encoding line of the second scan with the negative bipolar gradient pulse applied, then the second phase encoding line of

first scan with the positive bipolar gradient pulse again, then second phase encoding line of the second scan with the negative bipolar gradient pulse applied again, and so on. In the end, the positive bipolar gradient pulse is applied in acquiring all phase encoding lines of the first scan and the negative bipolar gradient pulse is applied in acquiring all phase encoding lines of the second scan. On the other hand, the proposed method option sets the number of scans acquired in a single acquisition to one. The polarity of the bipolar gradient pulse is alternated between phase encoding lines of the scan being acquired.

Flow Phantom Study

Transverse scans to measure water velocity along phantom tube were made using phase contrast and the proposed method. The flow phantom consisted of water flowing through a vinyl tube of 3/8" (9.525mm) inner diameter and 1/2" (12.7mm) outer diameter mounted to a digital gear pump (Cole-Palmer, IL, USA). The imaging parameters were: TR = 100ms, TE = 6.08ms, flip angle = 25°, matrix size = 128×128, voxel size = 0.8×0.8×5mm, encoding velocity υ_{enc} = 100cm/s. The pump flow rate was varied from 100ml/min (i.e. given 9.525mm inner flow tube diameter, this corresponds to a calculated flow velocity of 2.338993cm/s) to 1000ml/min (i.e. calculated flow velocity = 23.38993cm/s) at 100ml/min intervals. Water velocity measurements using phase contrast and the proposed method were made at each pump flow rate setting. Additionally, MR water velocity measurements were made at 50ml/min. For each flow rate setting on pump, three pairs of phase contrast scans were taken then later averaged, followed by three proposed method scans which were taken then later averaged also.

Phase contrast and proposed method water velocity values were compared to water velocity values computed from pump flow rate setting and tube cross section area. Paired student's *t*-test, correlation analysis and Bland-Altman analysis [24] were performed. The computed water velocity values were the gold standard. The inner diameter of the flow phantom's vinyl tube (0.9525cm) corresponds to a cross section area of 0.712557 cm^2. This requires approximately 111 image voxels of size 0.8×0.8×5mm to cover the area. Circular regions of interest (ROIs) covering the tube's inner diameter and containing approximately 111 voxels were drawn and water velocity values computed in each voxel. The mean of these velocity values gave the water velocity.

In Vivo Study

Transverse phase contrast and proposed method scans around the chin-mouth area were taken to measure blood velocity along the internal carotid artery (ICA) in seven volunteers. In each subject, interleaved cardiac phase scans that sample the cardiac flow profile at 100ms intervals were acquired in several cardiac cycles. The acquisitions were prospectively pulse gated. The relevant imaging parameters common to all acquisitions were: TR = 100ms, TE = 5.43ms, flip angle = 25° and encoding velocity υ_{enc} = 200cm/s. In a given volunteer, phase contrast and proposed method scans were acquired in tandem at the same slice location using the same imaging parameters. All acquisitions were repeated then later averaged.

Polygonal ROIs were drawn along the left and right ICA boundary. Blood velocity values were computed in each voxel. The mean of these velocity values gave the blood velocity along vessel. Maximum blood velocity values in the left and right ICA obtained by the proposed method were compared to corresponding maximum blood velocity values obtained by phase contrast. Paired student's *t*-test, correlation analysis and Bland-Altman analysis were performed on the maximum blood velocity values obtained by the two methods. Maximum blood velocity values obtained by phase contrast were taken to be the gold standard in the comparison because phase contrast has been validated in phantom, animal and human studies before [4-19].

Image Processing

Raw image data from the MRI scanner was processed offline using in-house software called mrflow. mrflow was written in MATLAB (The MathWorks Inc, Natick, Massachusetts, USA). mrflow uses header files that accompany the raw data for image reconstruction and calculating velocity maps. mrflow displays the subsequent magnitude images. mrflow determines velocity in hand drawn regions of interest by averaging velocity values in pixel locations within the regions of interest.

V. RESULTS

This chapter presents the main findings of this study. The results demonstrate that the proposed method is valid and that it reduces acquisition time. The *Phase Contrast and Proposed Method Validation in Phantom* section contains results that validate the implemented phase contrast and the proposed methods in phantom. The *In-vivo Proposed Method Validation* section contains results that validate the proposed method in vivo. The *Acquisition Time* section contains results that show the acquisition times of phase contrast and the proposed method in the in vivo study.

FIG. 4a and FIG. 4b show transverse magnitude images of the phantom vinyl tube taken from the same slice location using phase contrast and the proposed method respectively. FIG. 4c and FIG. 4d are in vivo transverse magnitude images around the chin-mouth area of one of the volunteers taken at the same slice location using phase contrast and the proposed method respectively. The phase encoding direction is in the vertical direction whereas the readout direction is in the horizontal direction. The proposed method images in FIG. 4b and FIG. 4d have the expected ghost image due to flow.

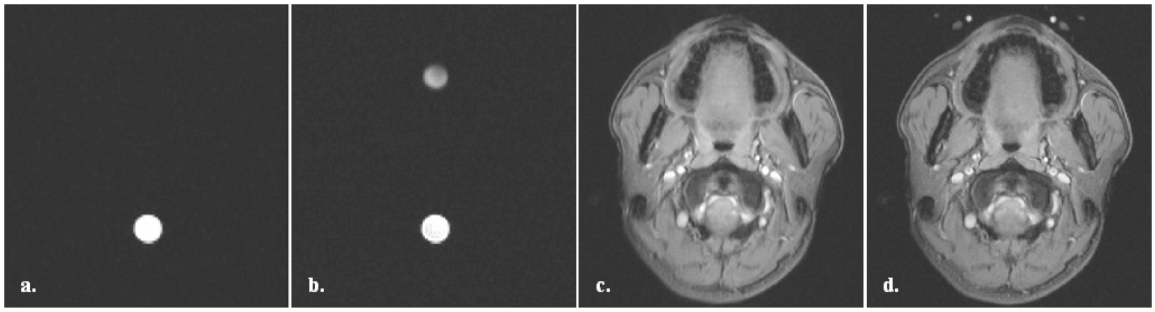

FIG. 4. (a) and (b) are transverse phase contrast and proposed method magnitude images of phantom respectively. (c) and (d) are transverse phase contrast and proposed method magnitude images around the same chin-mouth area of the same subject respectively.

Phase Contrast and Proposed Method Validation in Phantom

Water velocity along phantom tube measured by phase contrast and the proposed method were compared to water velocity calculated from pump flow rate setting and tube cross section area. Two-tail paired student's *t*-test of phase contrast and calculated water velocity values had p-value ($p < 0.148$) while two-tail paired student's *t*-test of the proposed method and calculated water velocity had p-value ($p < 0.161$). The correlation

coefficient between phase contrast and calculated water velocity values was 0.9998 whereas the correlation coefficient between the proposed method and calculated water velocity values was 0.9997 ($p < 0.001$). The mean difference between phase contrast and calculated water velocity values was -0.124cm/s with a 95% confidence interval ranging from -0.300cm/s to 0.052cm/s. The mean difference between proposed method and calculated water velocity values was 0.055cm/s with a 95% confidence interval ranging from -0.026cm/s to 0.137cm/s. FIG. 5. shows regression and Bland-Altman plots that compare phase contrast and proposed method water velocity values to calculated water velocity values.

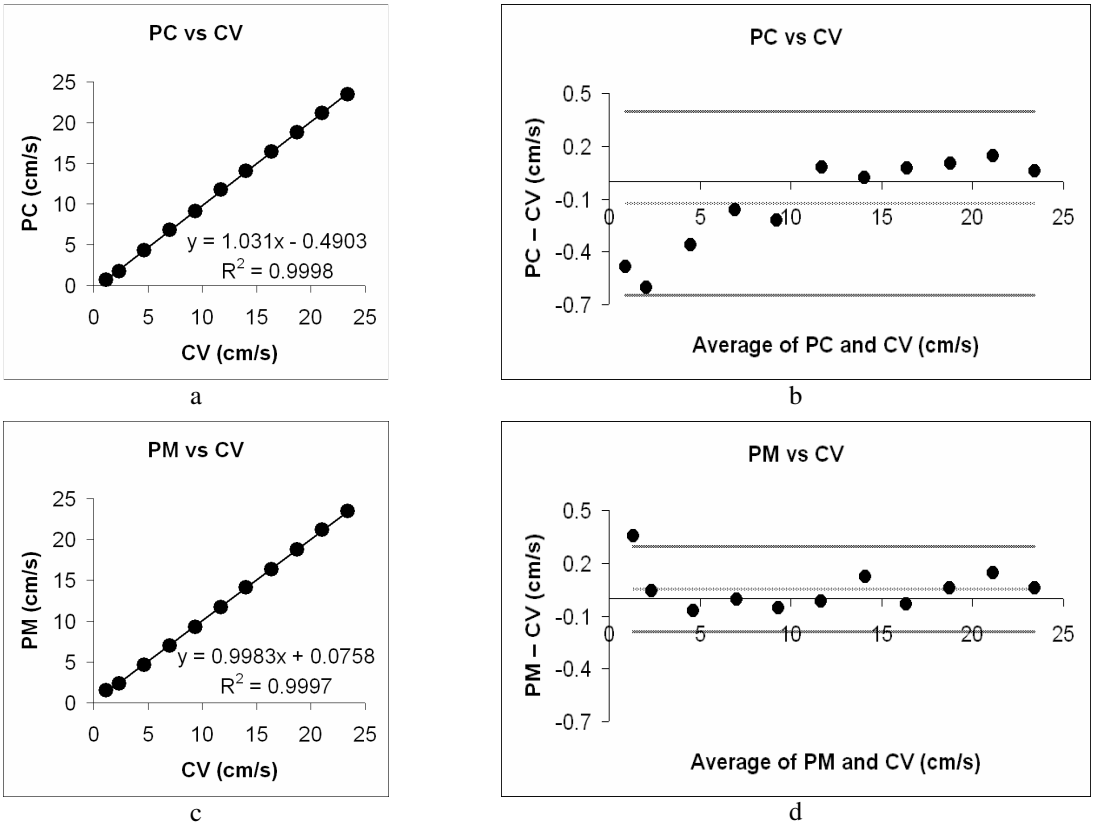

FIG. 5. Regression and Bland-Altman plots of phase contrast (PC) and proposed method (PM) water velocity along phantom tube versus calculated water velocity (CV). (a) regression plot of phase contrast water velocity along phantom tube, (b) Bland-Altman plot of phase contrast water velocity along tube, (c) regression plot of proposed method water velocity along phantom tube (d) Bland-Altman plot of proposed method water velocity in tube

In Vivo Proposed Method Validation

Left Internal Carotid Artery

FIG. 6 shows the blood velocity profile in the left internal carotid arteries of the seven volunteers within a cardiac cycle. Lines connected by green diamonds show blood velocity values obtained by phase contrast

whereas lines connected by red squares show blood velocity values obtained by the proposed method. The lines connected by blue triangles represent the proposed method blood velocity minus phase contrast blood velocity.

In the left internal carotid arteries of the seven volunteers, a two tail paired student's *t*-test of the phase contrast and the proposed method maximum blood velocity values gave p-value ($p < 0.720$). The correlation coefficient was 0.930 ($p < 0.001$) and the mean difference was 0.153cm/s with a 95% confidence interval ranging from -0.843cm/s to 1.148cm/s. FIG. 7 shows regression and Bland-Altman plots of phase contrast and the proposed method maximum blood velocity values in the left internal carotid arteries of the seven volunteers.

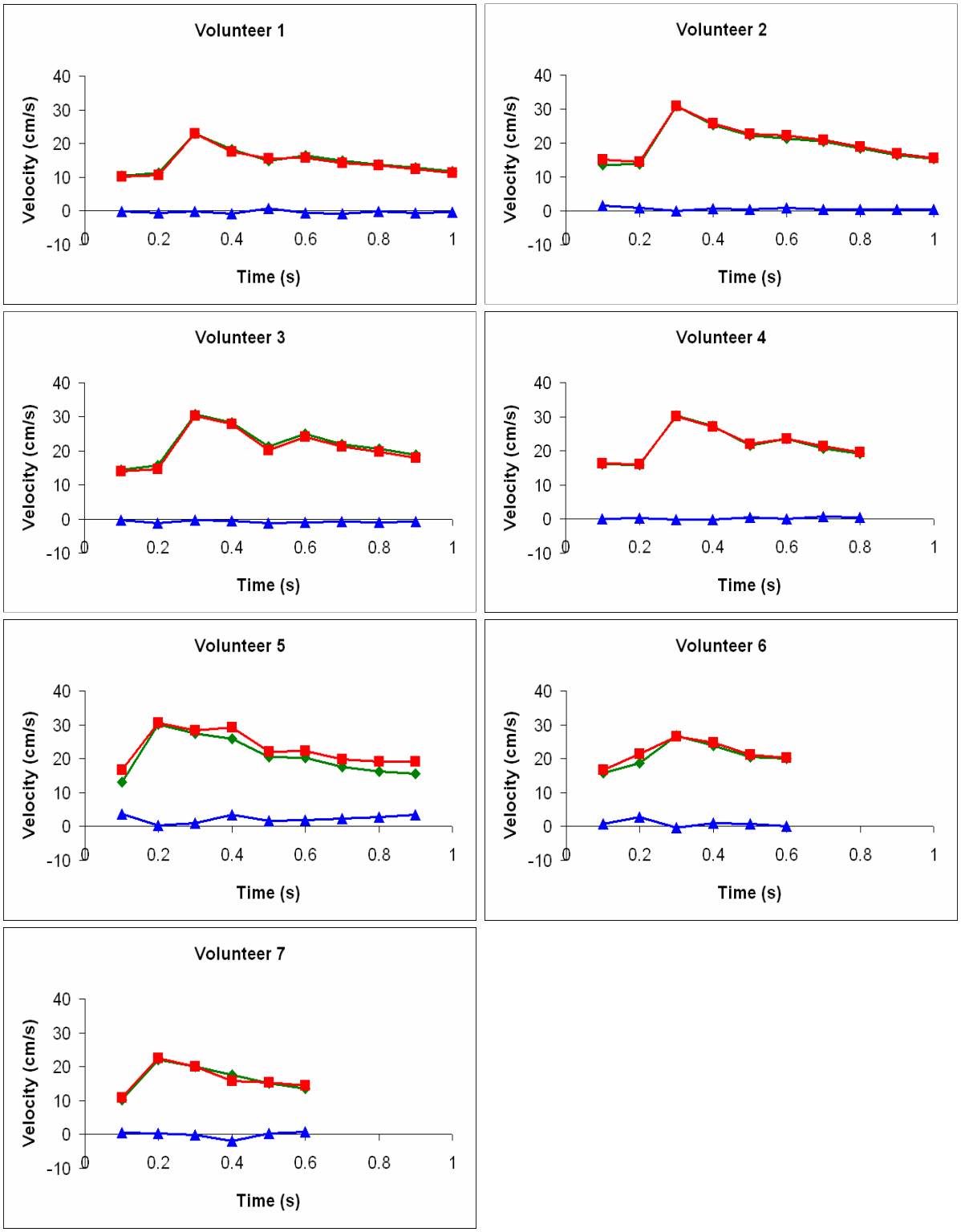

FIG. 6. Blood velocity profile in the left ICA of seven volunteers in one cardiac cycle. Lines connected by green diamonds represent the phase contrast velocity profile. Lines connected by red squares represent the proposed method velocity profile. Lines connected by blue triangles represent the proposed method velocity profile minus phase contrast velocity profile.

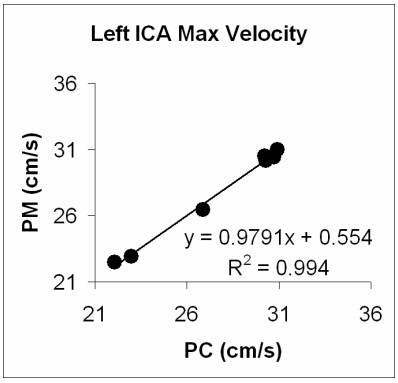

a

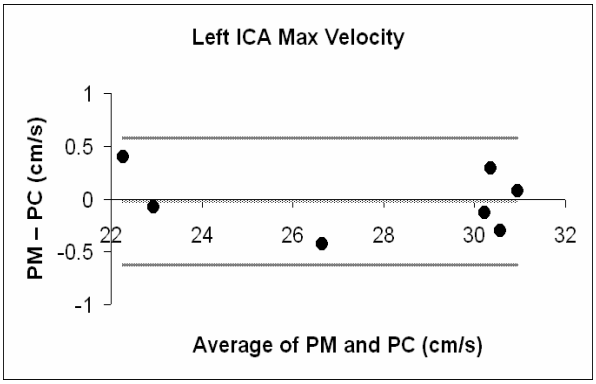

b

FIG. 7. (a) linear correlation between phase contrast and proposed method maximum blood velocity values in left ICA of seven volunteers. (b) the corresponding Bland-Altman plot of phase contrast and proposed method maximum blood velocity values in left ICA of the seven volunteers.

Right Internal Carotid Artery

FIG. 8 shows the blood velocity profile in the right internal carotid arteries of the seven volunteers within a cardiac cycle. Lines connected by green diamonds show blood velocity values obtained by phase contrast whereas lines connected by red squares show blood velocity values obtained by the proposed method. The lines connected by blue triangles represent the proposed method blood velocity values minus phase contrast blood velocity values.

In the right internal carotid arteries of the seven volunteers, a two tail paired student's *t*-test of the phase contrast and the proposed method maximum blood velocity values gave p-value ($p < 0.966$). The correlation coefficient was 0.985 ($p < 0.001$) and the mean difference was 0.020cm/s with a 95% confidence interval ranging from -1.072cm/s to 1.111cm/s. FIG. 9 shows regression and Bland-Altman plots of phase contrast and the proposed method maximum blood velocity values in the right internal carotid arteries of the seven volunteers.

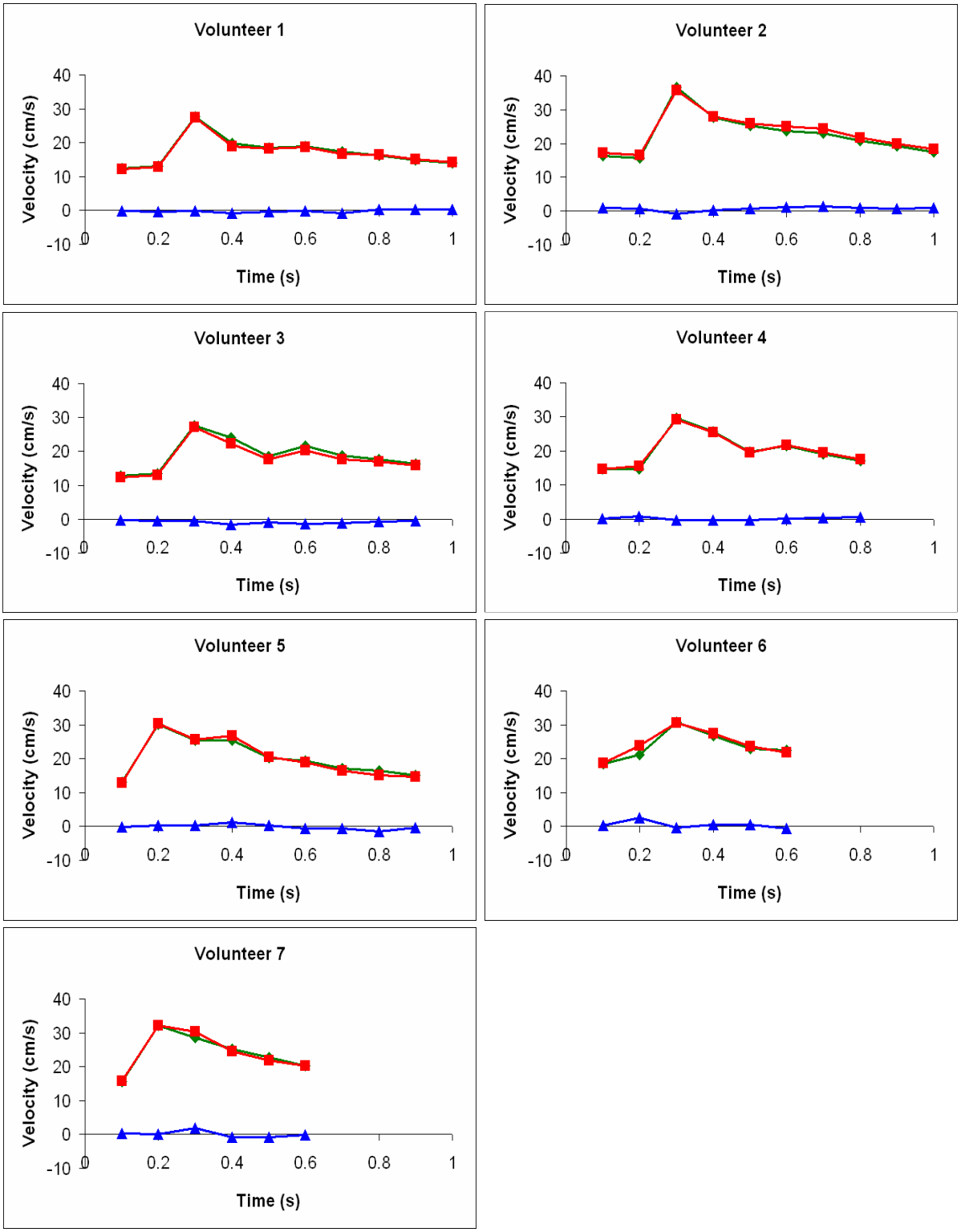

FIG. 8. Blood velocity profile in the right ICA of seven volunteers in one cardiac cycle. Lines connected by green diamonds represent the phase contrast velocity profile. Lines connected by red squares represent the proposed method velocity profile. Lines connected by blue triangles represent the proposed method velocity profile minus phase contrast velocity profile.

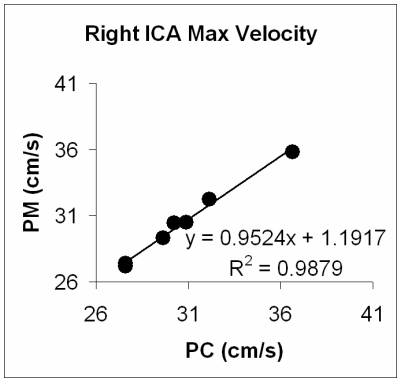

a

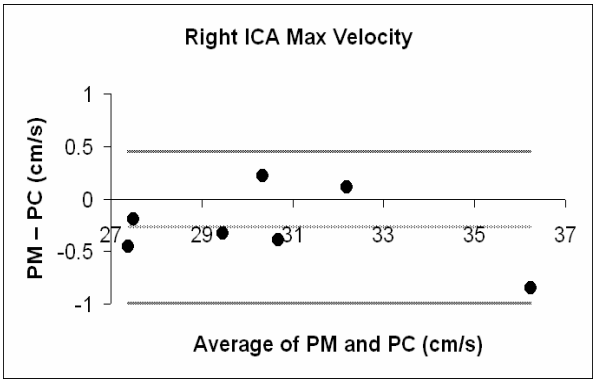

b

FIG. 9. (a) linear correlation between phase contrast and proposed method maximum blood velocity values in right ICA of seven volunteers. (b) the corresponding Bland-Altman plot of phase contrast and proposed method maximum blood velocity values in right ICA of the seven volunteers.

Acquisition Time

Table 1 below shows the total acquisition time using phase contrast and the proposed method in the seven volunteers.

	Total Acquisition Time (s)	
	Phase Contrast	Proposed Method
Volunteer 1	1121	575
Volunteer 2	823	423
Volunteer 3	1220	584
Volunteer 4	952	521
Volunteer 5	724	377
Volunteer 6	818	392
Volunteer 7	745	388

TABLE 1. Total scan acquisition time for the seven volunteers.

VI. DISCUSSION

Interpretation of Results

The phantom study results showed no significant difference ($p<0.161$), a high correlation coefficient ($r^2=0.9997$) and a low mean difference (0.055cm/s) between the proposed method and calculated water velocity values. In vivo study results showed no significant difference (left ICA: $p<0.720$, right ICA: $p<0.966$), a high correlation coefficient (left ICA: $r^2=0.9302$, right ICA: $r^2=0.9846$) and a low mean difference (left ICA: 0.153cm/s, right ICA: 0.020cm/s) between the proposed method and phase contrast maximum blood velocity values. However, velocity values obtained by the proposed method intrinsically contain minute errors because the background signal onto which the flow ghost is overlaid is assumed to be zero in Eq. [9]. Also, in the in vivo study, the cardiac phases were acquired in an interleaved manner. The accuracy of the blood velocity measurements depends on the cardiac flow profile remaining constant throughout acquisition. Any actual or noise induced beat to beat variations registered on the gating device adversely affect blood flow velocity measurements [21].

Acquisition Time

The proposed method required only one scan to quantify velocity. Thus, the proposed method acquisition time was about half that of phase contrast. However, all in vivo scans were prospectively gated and thus scan acquisition time depended on heart rate. Any heart rate variation during scan acquisition affected acquisition time. This explains why the proposed method acquisition time is not exactly half that of phase contrast.

Field of View Configuration

The left and right ICAs are located near the center of field of view with respect to the phase contrast direction. This eliminated the need to rotate and/or increase the field of view in the phase encoding direction so as to provide room for the proposed method flow ghost. Therefore, the same field of view was used in corresponding phase contrast and proposed method scans in subjects.

Given in the localizer image, a field of view that inscribes the object being imaged and a region of interest where flow is to be quantified, it is possible to formulate an algorithm that automatically configures the field of view for minimum acquisition time. Basically, the algorithm rotates, translates and increases the inscribing field of view so as to move the region of interest near the center with respect to the phase encoding direction. The field of view is then increased accordingly in the phase encoding direction so as to provide room for the proposed method flow ghost. The sampling matrix is adjusted accordingly so as to maintain spatial resolution.

Doubling the length of the inscribing field of view in the phase encoding direction and increasing the sampling matrix accordingly will create enough room for all possible proposed method flow ghosts while maintaining spatial resolution. This makes it possible to quantify velocity in all regions of interest. But, the proposed method acquisition time in this case is equal to that of phase contrast having two scans with only half the field of view and half the sampling matrix. Therefore, while maintaining spatial resolution, the least optimal field of view configuration should be the one that results in the proposed method acquisition time being equal to that of phase contrast.

The size of the field of view is limited by the MRI scanner bore size. It may not be possible to increase the field of view in the phase encoding direction in a situation where the object being imaged tightly fits in the scanner. This problem is resolved by oversampling in the phase encoding direction appropriately rather than actually increasing the field of view in the phase encoding direction.

Rapid Flow Quantification

Adapting the propose method to rapid imaging methods such as Interleaved Echo Planar Imaging sequence (IGEPI) [25, 26] can improve the temporal resolution of cardiac phases acquired. The proposed method can be adapted to IGEPI by reversing the bipolar gradient pulse between k-space segments as in FIG. 10. FIG. 10 shows k-space trajectories example for IGEPI in which only two interleaved segments marked by 1 and 2 are shown. A positive bipolar gradient pulse is applied in acquiring phase encoding segments marked + whereas a negative bipolar gradient pulse is applied in acquiring phase encoding segments marked –. The objective is to have alternating +, – k-space lines in the phase encoding (PE) direction. RO is the readout direction.

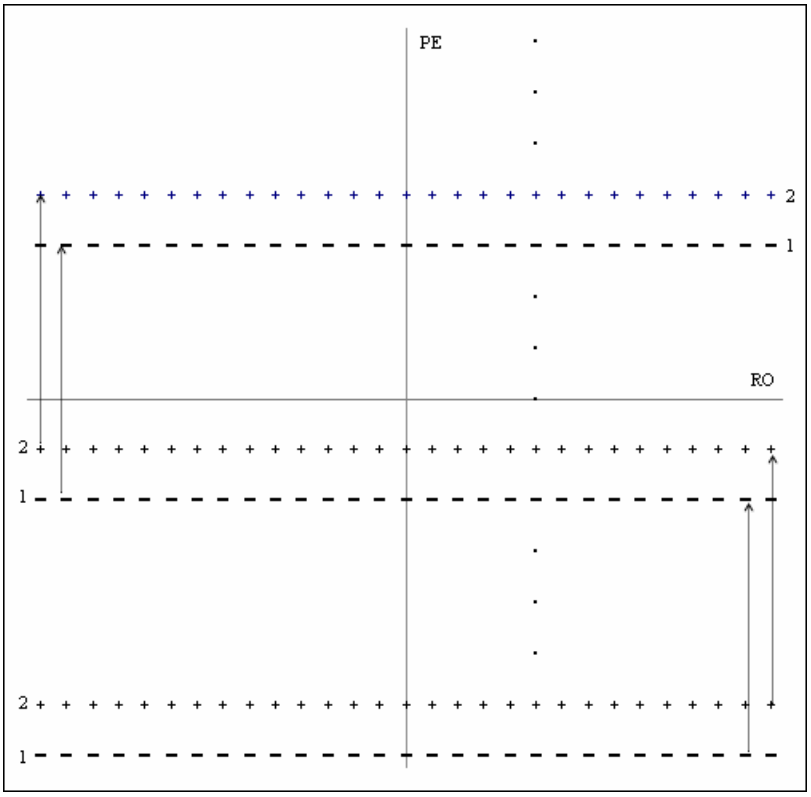

FIG. 10. Proposed method k-space trajectories example for IGEPI in which only two interleaved segments marked by 1 and 2 are shown.

VII. CONCLUSION

In the phantom study, the proposed method correlates well with calculated velocity values (r^2=0.9997) with very small mean difference (0.055cm/s). In the in vivo study, the proposed method maximum blood velocity values correlates well with the phase contrast blood velocity values (left ICA: r^2=0.9302, right ICA: r^2=0.9846) with very small mean difference (left ICA: 0.153cm/s, right ICA: 0.020cm/s). The proposed method quantifies velocity in a region of interest identified in localizer image prior to scanning. Given the same spatial resolution, the proposed method acquisition time is about half that of phase contrast in the best case scenario and equal to that of phase contrast in the worst case scenario. The proposed method can be adapted into rapid imaging methods and thus improve temporal resolution. The proposed method can be easily implemented, requires minimum processing of data collected and doesn't require special hardware.

REFERENCES

1. Evans, A.J., et al., *Magnetic resonance imaging of blood flow with a phase subtraction technique. In vitro and in vivo validation.* Invest Radiol, 1993. **28**(2): p. 109-15.

2. Pelc, L.R., et al., *Arterial and venous blood flow: noninvasive quantitation with MR imaging.* Radiology, 1992. **185**(3): p. 809-12.

3. Pelc, N.J., et al., *Phase contrast cine magnetic resonance imaging.* Magn Reson Q, 1991. **7**(4): p. 229-54.

4. Bogren, H.G., et al., *Quantitation of antegrade and retrograde blood flow in the human aorta by magnetic resonance velocity mapping.* Am Heart J, 1989. **117**(6): p. 1214-22.

5. Bogren, H.G., et al., *Pulmonary artery distensibility and blood flow patterns: a magnetic resonance study of normal subjects and of patients with pulmonary arterial hypertension.* Am Heart J, 1989. **118**(5 Pt 1): p. 990-9.

6. Chatzimavroudis, G.P., et al., *Evaluation of the precision of magnetic resonance phase velocity mapping for blood flow measurements.* J Cardiovasc Magn Reson, 2001. **3**(1): p. 11-9.

7. Firmin, D.N., et al., *In vivo validation of MR velocity imaging.* J Comput Assist Tomogr, 1987. **11**(5): p. 751-6.

8. Kilner, P.J., et al., *Valve and great vessel stenosis: assessment with MR jet velocity mapping.* Radiology, 1991. **178**(1): p. 229-35.

9. Kilner, P.J., et al., *Magnetic resonance jet velocity mapping in mitral and aortic valve stenosis.* Circulation, 1993. **87**(4): p. 1239-48.

10. Langerak, S.E., et al., *MR flow mapping in coronary artery bypass grafts: a validation study with Doppler flow measurements.* Radiology, 2002. **222**(1): p. 127-35.

11. Maier, S.E., et al., *Human abdominal aorta: comparative measurements of blood flow with MR imaging and multigated Doppler US.* Radiology, 1989. **171**(2): p. 487-92.

12. Meier, D., S. Maier, and P. Bosiger, *Quantitative flow measurements on phantoms and on blood vessels with MR.* Magn Reson Med, 1988. **8**(1): p. 25-34.

13. Pettigrew, R.I., et al., *Quantitative phase-flow MR imaging in dogs by using standard sequences: comparison with in vivo flow-meter measurements.* AJR Am J Roentgenol, 1987. **148**(2): p. 411-4.

14. Powell, A.J., et al., *Phase-velocity cine magnetic resonance imaging measurement of pulsatile blood flow in children and young adults: in vitro and in vivo validation.* Pediatr Cardiol, 2000. **21**(2): p. 104-10.

15. Sakuma, H., et al., *Quantification of coronary artery volume flow rate using fast velocity-encoded cine MR imaging.* AJR Am J Roentgenol, 1997. **168**(5): p. 1363-7.

16. Shibata, M., et al., *Assessment of coronary flow reserve with fast cine phase contrast magnetic resonance imaging: comparison with measurement by Doppler guide wire.* J Magn Reson Imaging, 1999. **10**(4): p. 563-8.

17. Simpson, I.A., et al., *Cine magnetic resonance imaging for evaluation of anatomy and flow relations in infants and children with coarctation of the aorta.* Circulation, 1988. **78**(1): p. 142-8.

18. Szarf, G., et al., *Zero filled partial fourier phase contrast MR imaging: in vitro and in vivo assessment.* J Magn Reson Imaging, 2006. **23**(1): p. 42-9.

19. Van Rossum, A.C., et al., *An in vivo validation of quantitative blood flow imaging in arteries and veins using magnetic resonance phase-shift techniques.* Eur Heart J, 1991. **12**(2): p. 117-26.

20. Klein, C., et al., *Magnetic resonance flow measurements in real time: comparison with a standard gradient-echo technique.* J Magn Reson Imaging, 2001. **14**(3): p. 306-10.

21. Gatehouse, P.D., et al., *Real time blood flow imaging by spiral scan phase velocity mapping.* Magn Reson Med, 1994. **31**(5): p. 504-12.

22. Debatin, J.F., et al., *Renal artery blood flow: quantitation with phase-contrast MR imaging with and without breath holding.* Radiology, 1994. **190**(2): p. 371-8.

23. Haacke, E.M., *Magnetic resonance imaging : physical principles and sequence design*. 1999, New York: J. Wiley & Sons. xxvii, 914 p.

24. Bland, J.M. and D.G. Altman, *Statistical methods for assessing agreement between two methods of clinical measurement.* Lancet, 1986. **1**(8476): p. 307-10.

25. McKinnon, G.C., et al., *Interleaved echo planar flow quantitation.* Magn Reson Med, 1994. **32**(2): p. 263-7.

26. McKinnon, G.C., *Interleaved echo planar phase contrast angiography.* Magn Reson Med, 1994. **31**(6): p. 682-5.